Light regulation of organic light-emitting diodes with conductive distributed Bragg reflectors

Yun Hu, Jing-song Huang, Paul Stavrinou, Donal D. C. Bradley

Yun Hu, Jing-song Huang, Paul N. Stavrinou, Donal D. C. Bradley, "Light regulation of organic light-emitting diodes with conductive distributed Bragg reflectors," Proc. SPIE 12314, Optoelectronic Devices and Integration XI, 123140O (20 December 2022); doi: 10.1117/12.2641624

SPIE.

Event: SPIE/COS Photonics Asia, 2022, Online Only

Light regulation of organic light-emitting diodes with conductive distributed Bragg reflectors

Yun Hu[a], Jing-song Huang*[a], Paul N Stavrinou*[a,b], Donal D C Bradley*[a]
[a]Oxford Suzhou Centre for Advanced Research (OSCAR), University of Oxford, 388 Ruo Shui Road, Suzhou Industrial Park, Jiangsu, 215123, P.R. China; [b]Department of Engineering Science, University of Oxford, Oxford OX1 3PJ U.K.
*Corresponding authors

ABSTRACT

Non-metallic mirror, such as semiconductor distributed Bragg reflectors (DBRs), has been widely integrated in the structure of optoelectronic devices. However, constructing conductive DBR in organic optoelectronic device is still scarce, because of the incompatibility of high-temperature processes in the preparation of inorganic DBR. Herein, it is confirmed that organic-oxide hybrid DBR can achieve high conductivity and light manipulation. When thermal evaporated material MoO3 is doped into organic material (1,1-bis[4-[N,N-di(p-tolyl)amino]phenyl]cyclohexane, TAPC), the conductivity of TAPC can be increased by ten thousand times with very small refractive index change. It is shown that 8.5 pairs DBR at 460 nm has a reflectivity of about 95%, and the driving voltage is 8.2 V at the current density of 100 mA cm^{-2}. Then, a transparent organic light-emitting diode with integrated bottom conductive DBR are fabricated to confirm the functionality of light regulation. Our results confirm that integrated optoelectronic devices with DBR as reflector can be achieved with low operating voltage.

Keywords: conductive distributed Bragg reflector, OLED, thermally activated delayed fluorescence

1. INTRODUCTION

Distributed Bragg reflector (DBR) has excellent optical control characteristics, such as adjustable wavelength, controllable reflectivity, and is widely used in semiconductor devices.[1-5] It is reported that the dielectric DBR used in optoelectronic devices is mostly made of SiO2, ZrO2, MgF2 or other oxide materials, and the refractive index of these materials is about 1.5-2.5.[6] In addition, they are prepared by high power consumption equipment such as electron-beam (EB) evaporation and pulsed laser deposition (PLD). In optoelectronic devices, DBR has been used to adjust the semi-transmissive photovoltaic cells or to prepare light-emitting diodes (LEDs) with microcavity structure.[7,8]

In vertical-cavity surface-emitting lasers (VCSELs) devices, the application of conductive DBR (AlGaAs/GaAs based DBRs) not only has wavelength selective control, but also can adjust electrical characteristics.[9] And conductive DBR often selects III-group elements, such as Al, Ga, In, and Sn for doping.[10] Since the preparation process of inorganic materials requires high temperature processing and lattice matching, they are not suitable for organic optoelectronic devices. Therefore, researchers have developed other novel DBR structures of organic or organic-inorganic hybrid systems with electrical characteristics. For example, alternating current (AC)-driven

Optoelectronic Devices and Integration XI, edited by Xuping Zhang, Baojun Li, Changyuan Yu, Xinliang Zhang,
Proc. of SPIE Vol. 12314, 123140O · © 2022 SPIE · 0277-786X · doi: 10.1117/12.2641624

electroluminescent devices with printed inorganic/organic hybrid dielectric mirrors (CuSCN/CA)CuSCN; direct current (DC)-driven polymer LEDs with the poly(p-phenylene vinylene)-silica composite material for DBR.[11, 12] Some DBR devices based on thermal evaporation of small molecule semiconductor materials have been proposed, including 4,4′-Bis[4-(diphenylamino)styryl]biphenyl (BDAVBi)/2-(4-biphenyl)-5-(4-tert-butylphenyl)-1,3,4-oxadiazole (PBD) doped with Perfluorotetracosane (C24F50), MoO3/4,4′,4′′-tris[3-Methylphenyl(phenyl)-amino]triphenylamine (m-MTDATA)/ 1,4,5,8,9,11-hexaazatriphenylene-hexacarbonitrile (HAT-CN).[13, 14] These DBRs grown on Indium tin oxide (ITO) substrates can effectively obtain high performance compared to growing transparent electrodes (such as ITO) on DBRs, which usually causes the destruction of the DBR structure. Therefore, the most challenging thing of integrating a conductive DBR into an organic optoelectronic device is to reduce the driving voltage.

Generally, methods for improving the conductivity of thin films in organic optoelectronic devices include optmizing the molecular stacking, metal doping (Li, Cs), metal oxide doping (MoO3/WO3/V2O5), and organic small molecule doping (F4-TCNQ/HATCN).[15-19] Among them, metal oxide doping is widely used in organic light-emitting diode (OLED) devices, which can reduce the interface injection barrier and improve the conductivity of the doped film. The charge generation efficiency of metal oxide dopants is mainly confined by the dispersion features in organic semiconductors, which means that the dopant deposition process and doping ratio are significant factors that need to be considered.[20] The refractive index of the organic component of the doped film is often between 1.6-1.9, and the refractive index of the metal oxide dopant is between 1.7-2.3.[21, 22] Theoretically, by adjusting the doping ratio, a tunable value of refractive index between organic and metal oxides can be obtained, but the preparation process is full of challenges.

In this work, we use thermal deposition technique for the realization of conductive DBR with MoO3 and doped organic material 1,1-bis[(di-4-tolylamino)phenyl]cyclohexane (TAPC): MoO3 as component materials. MoO3 is a widely used n-type material (Eg = 3.1 eV) with high ionic conductivity, and TAPC is a commonly used hole transporting material in OLEDs. For TAPC: MoO3 (20 wt.%) film, its conductivity reached to 0.8×10-4 S/m, close to that of the MoO3 (2×10-4 S/m), and the conductivity of the prepared DBR also reached to 0.6×10 -4 S/m. The reflectivity of 8.5 pairs DBR reaches to 82.5% with the full width at half maximum (FWHM)@560 nm = 96.4 nm, and 95% with the FWHM@460 nm = 75.7 nm. Furthermore, we fabricate the conductive DBR between the two electrodes of the OLEDs as an optical adjustment mirror, which can reduce the surface plasmon polariton (SPP) effect, compared to the metal electrode as the mirror.[23] The blue device with DBR has a driving voltage as low as 4.2 V, and FWHM is reduced by half compared to that of the device without DBR. Our results confirm that conductive DBR as an optical mirror can adjust the light intensity of bottom emission and top emission as required.

2. RESULTS AND DISCUSSION

We measured the refractive index of MoO3, TAPC and the doping layer, as shown in Figure 1a. The refractive index of these doped layers has similar values about 1.65 -1.85 in the visual light spectral region, while that of MoO3 is about 2.0 - 2.3. It indicates that TAPC: MoO3 and MoO3 layers can act as the low and high refractive index films in DBR structure, respectively. Even if the doping mass ratio of MoO3 is increased, the refractive index of the TAPC doped film does not change much, because of the high density ratio of MoO_3/TAPC. This also provides convenience for the control of the film thickness. The doped film has charge transfer absorption peak at about 700 nm, which

would have adverse side effects for the reflectance of DBRs.[24] Then, we confirm the electrical conductivity of each layer of the films. Figure 1b shows the current density-voltage curves of hole-only devices with thickness of 120 nm. With the doping ratio increased of MoO_3, the conductivity of doped films is close to that of a pure MoO_3 film, which is about 2×10^{-4} S m^{-1} as shown in Figure 1c.[14]

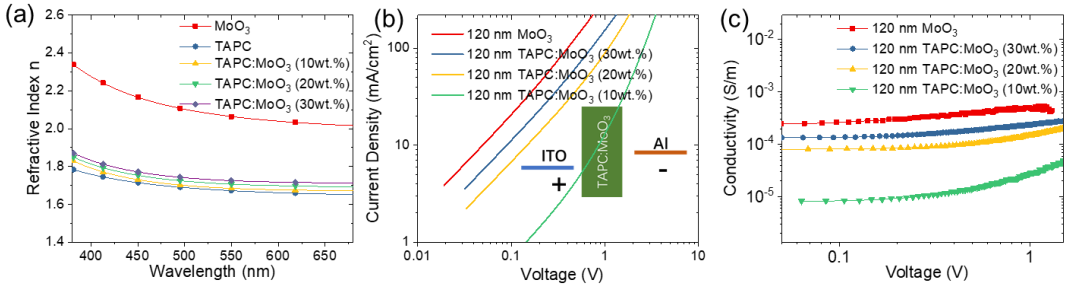

Figure 1. (a) Refractive index n of MoO3, TAPC and doped films on silicon wafer were measured with ellipsometer. The comparative (b) current density-voltage and (**c**) conductivity-voltage characteristics of hole-only devices based on MoO3 and TAPC doped films. The insert in (b) shows the schematic diagram of device structure.

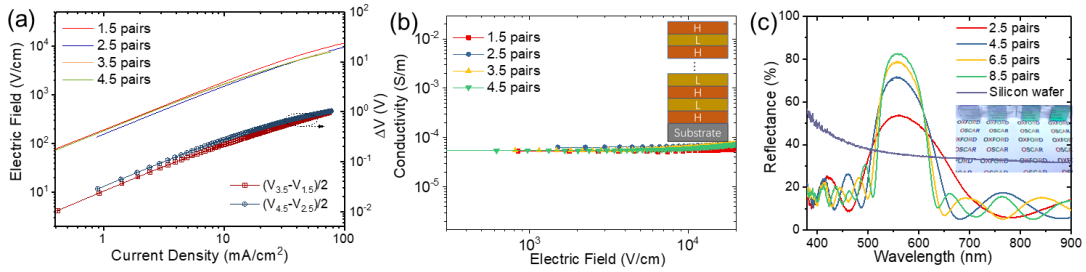

Figure 2. (a) The current density-electric field-voltage drop (△V) and (b) conductivity-electric field curves of hole-only devices. The repetition period varies from 1.5 to 4.5. (c) Reflectance of DBR films on quartz with incident ray at 5°. The central wavelength of DBRs is at 560 nm. The thickness of MoO3 is 68 nm and TAPC: 20 wt.% MoO3 is 82 nm.

Obviously, high conductivity and refractive index contrast of layers are the key parameters for achieving high performance DBR. To demonstrate, we fabricated the different period of DBRs as shown in Figure 2. The maximum reflection of the DBRs is at 560 nm, equivalently, the thickness of MoO_3 is 67 nm and TAPC: 20 wt.% MoO_3 is 82 nm, which is a quarter of the central wavelength of the designed DBR. The results of current density-electric field-voltage drop (△V) are plotted in Figure 2a. The voltage drop of a single pair of DBR is about 0.25V at 10 mA/cm2. With increasing the current density, electric field strength exhibits a linear increase. It suggests that the conductivity of DBRs remains the same, which are calculated in the Figure 2b. The DBR structure shows similar conductive properties compared with single-layer films. Figure 2c shows the reflectance spectra of the DBRs on the quartz substrate. The maximum reflectance is 82.5% for 8.5 pairs and the FWHM is about 96 nm.

In order to verify the accuracy control of film thickness, we also prepared 8.5 pairs DBRs with center wavelengths at 460 nm, 540 nm and 550 nm shown in Figure 3. For comparison, the maximum reflectance of these DBRs on quartz substrates are 94.8% at 460 nm, 86.5% at 540 nm and 84.2% at 550 nm, respectively, while reflectance of DBRs on ITO substrates seems as good as on quartz substrates. With the blue shift of the center wavelength, the reflectance increases

correspondingly, which is due to the enhancement in the refractive index contrast and the weakening of charge transfer absorption effect of component layers. The simulation results of the blue DBR exhibit consistency in the reflectance spectrum as shown in Figure 3a. Then, the doped semiconducting DBRs with the structure of ITO/8.5 pairs DBRs /Al (100 nm) were further fabricated. The current density-voltage curves of the hole only devices are shown in Figure 3b,d,f. The driving voltage of the 8.5 pairs DBRs are 8.3 V, 9.6 V and 10.3 V for central wavelength at 460 nm, 540 nm and 550 nm at 100 mA cm^{-2}, respectively. These voltage values are close to the results calculated using the electric field strength of Figure 2a.

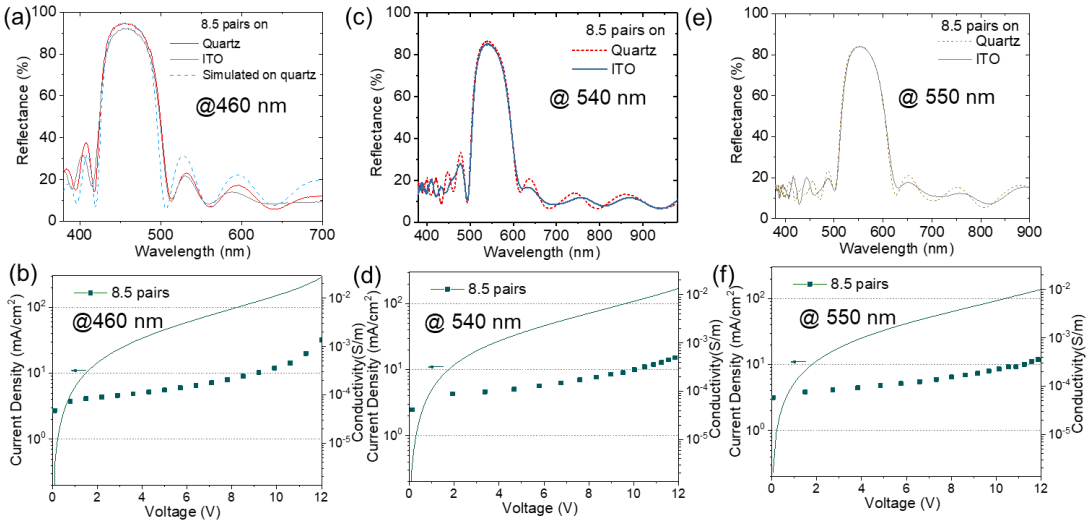

Figure 3. (a, c, e) Reflectance of DBR films on quartz and ITO substrates with incident ray at 5°. (b, d, f) The current density-voltage-conductivity curves of the hole only devices with 'ITO/ 8.5 pairs DBR /Al' structure. For DBR at 460 nm, the thickness of MoO3 is 53.5 nm and TAPC: 20 wt.% MoO3 is 65.9 nm. For DBR at 540 nm, the MoO3 is 65.2 nm, and TAPC:MoO3 (20 wt.%) is 79 nm. For DBR at 550 nm, the MoO3 is 66.6 nm, and TAPC:MoO3 (20 wt.%) is 80.6 nm.

Based on these results, we fabricated OLEDs with integrated conductive DBR in devices. Usually, the peak position of the photoluminescence (PL) spectrum of the emitter is not ideal. Therefore, adjusting the emission wavelength and efficiency of OLED devices through the reflection characteristics of DBR can satisfy actual requirements. For the comparison, we designed green and blue devices with different thermally activated delayed fluorescence (TADF) dyes as emitters. The specific device structures are as follows.

Green OLED without DBR (Device G1): ITO (135 nm)/MoO3(3 nm) / mCP (45 nm)/mCP: 4CZIPN (8 wt.%, 20 nm)/TmPyPb (45 nm)/LiF (1 nm)/Al (2 nm)/Ag (16.5 nm)/MoO3 (40 nm)

Green OLED with 8.5 pairs DBR (Device G2): ITO (135 nm)/DBR films (@550nm) / MoO3(3 nm) / mCP (45 nm)/mCP: 4CZIPN (8 wt.%, 20 nm)/TmPyPb (45 nm)/LiF (1 nm)/Al (2 nm)/Ag (16.5 nm)/MoO3 (40 nm)

Blue OLED without DBR (Device B1): ITO (135 nm)/MoO3(3 nm) / TCTA (30 nm)/ mCP (15 nm) DPEPO: TDBA-Ac (20 wt.%, 20 nm)/ DPEPO (10 nm)/Bphen (35 nm)/LiF (1 nm)/Al (2 nm)/Ag (16.5 nm)/MoO3 (35 nm)

Blue OLED with 8.5 pairs DBR (Device B2): ITO (135 nm)/DBR films (@460nm) / MoO3(3 nm) / TCTA (30 nm)/ mCP (15 nm) DPEPO: TDBA-Ac (20wt.%, 20 nm)/ DPEPO (10 nm)/Bphen (35 nm)/LiF (1 nm)/Al (2 nm)/Ag (16.5 nm)/MoO3 (35 nm)

There are slightly discrepancies of capping layer (MoO3) thickness between green and blue devices. Usually, the thickness of capping layer will influence the position of the maximum transmission peak. Figure 4a, b shows the energy-level diagrams of devices, wherein the conductive DBR function as a hole transporting layer and a mirror for reflected spectrum control. In these devices, ultra-thin aluminum (2 nm) as seed layer is used to reduce the sheet resistance and surface roughness.[25] With optimized materials and optical thickness condition, we fabricated p-i-n structure devices and measured their performances. The devices without conductive DBRs show the similar EL peaks from bottom and top emission at 5 mA $cm^{-2}$for G1 and B1 (Figure 4c, e), which correspond to the PL spectra with the same doping ratio. A little difference of EL spectra in shape probably causes by the transmittance of electrode. After DBR is introduced into the device, the emission spectrum of the device has undergone a huge change, which not only causes the position of the emission peak to shift, but the spectral shape is also affected by the bandwidth of the DBR. Figure 4d shows the top emission peak at 538 nm for G2, and 500 nm from bottom emission. Similarly, for the B2 device (Figure 4f), the emission peak positions are at 459 and 510 nm, corresponding to top and bottom emission, respectively. Due to the high reflection characteristics of DBRs, the devices have weak microcavity effect, and the corresponding FWHM of top emission is halved. When we increase the driving voltage, the spectra of top emission from G2 and B2 remain the same. For the top emission of B2 device, we carried out an optical simulation, which is consistent with the experimental result. It indicates that the thickness of each layer is controlled accurately. As the variation of TCTA and Bphen within 1st order cavity thickness, the peak wavelength has a red shift with increasing the thickness as shown in Figure5. Finally, by designing the thickness of the DBR and the functional layers, the emission peak of the OLEDs can be controlled within the PL spectral range.

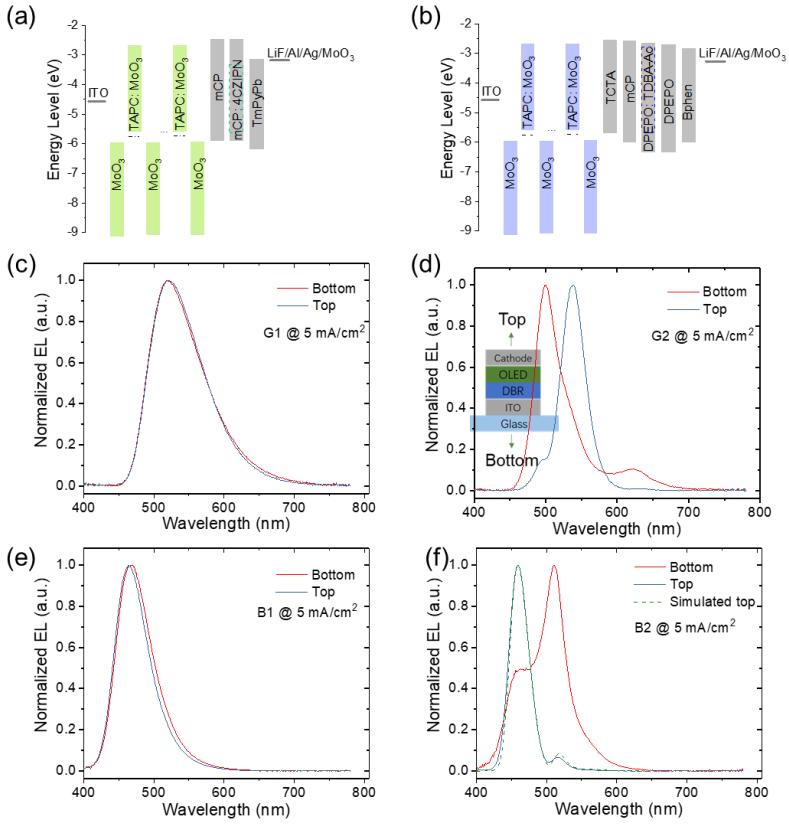

Figure 4. Energy-level diagrams of (a) green, and (b) blue devices. (c-f) The electroluminescence (EL) spectra of

green and blue OLEDs. The inset in (d) shows the direction of emission.

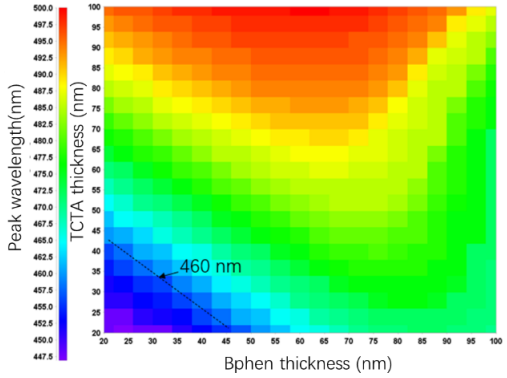

Figure 5 The peak wavelength relate to TCTA and Bphen thickness.

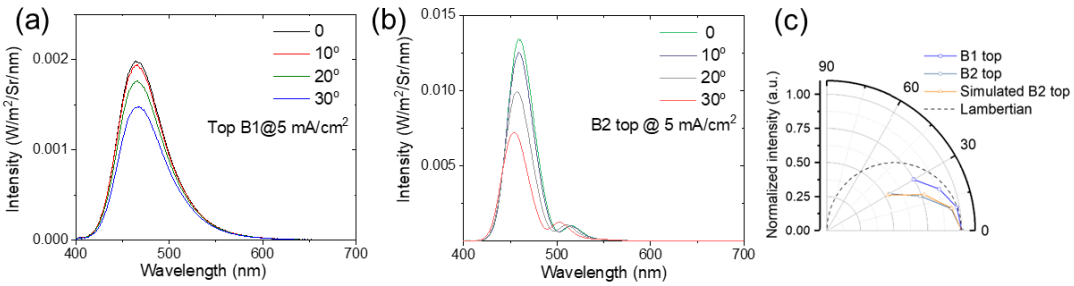

Figure 6. Angle-dependent electroluminescence (EL) spectra of blue OLED. (a, b) EL spectra measured at different angles. (c) Comparison of the angle-dependent EL intensity and the standard Lambertian distribution.

Angle-dependent electroluminescence (EL) spectra of blue OLEDs from top side is shown in Figure 6. The peak position of B2 has 6 nm blue-shifte with the change of the light output angle of 30 degrees compared with that of 1-2 nm of B1 device (Figure 6a, b). This difference is due to the blue shift of the center wavelength of DBR. In Figure 6c, we compared the angle dependent EL intensity with the standard Lambertian distribution. The experimental result of B2 is consistent with the simulation result. It is proved that the OLED device with DBR tends to emit in the forward direction.

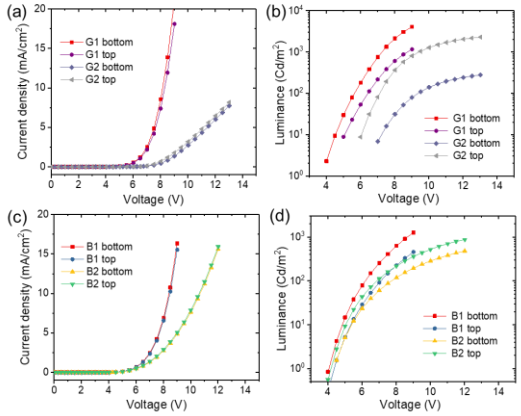

Figure 7. (a,c) J-V and (b, d) L-V characteristics of double-sided green and blue OLEDs.

Table 1 The summary of device performances.

Device		EL peak (nm)	FWHM (nm)	CIE (X,Y) @ 5 mA cm^{-2}	Current Efficiency (cd/A)	Power Efficiency (lm/W)
Device G1	Bottom	518	89	(0.312, 0.575)	35.02	25.54
	Top	519	89	(0.309, 0.579)	11.30	7.08
Device G2	Bottom	500	45	(0.212, 0.526)	7.34	3.12
	Top	538	40	(0.256, 0.682)	65.35	31.51
Device B1	Bottom	470	61	(0.141, 0.169)	13.94	10.91
	Top	464	57	(0.140, 0.144)	5.32	4.17
Device B2	Bottom	511	52	(0.154, 0.356)	5.94	4.13
	Top	460	32	(0.141, 0.065)	9.72	7.6

We also investigate the current density-voltage (J-V) and luminance-voltage (L-V) characteristics of the four devices as shown in Figure 7. Due to the bulk resistance effect of the DBRs, the increase of current density slows down with the increase of voltage, relative to the devices without DBRs. Note that the bottom and top brightness of the devices have been reversed with the insertion of the DBRs. Table 1 summarizes the device performances and Commission International de lEclairage (CIE) of spectra. To evaluate the time and temperature stability of the conductive DBRs, we performed a series of measurement. The results show that after a week of aging at nitrogen atmosphere, the optical and electrical performance of DBR has a slight degradation. The reason for the degradation is the diffusion of MoO_3 from high concentration to low concentration layer. Furthermore, excessively high temperature (i.e., exceeding the glass transition temperature) will crack the surface. Therefore, increasing the stability of the DBR composition can resist the destruction of Joule heat generated by high current density.

3. EXPERIMENTAL

Materials: All chemicals and materials were purchased from Xi'an Polymer Light Technology Co. and Luminescence Technology Co. The chemical materials used in OLEDs are molybdenum trioxide (MoO3), 1,1-bis[(di-4-tolylamino)phenyl]cyclohexane (TAPC), 4,4',4"-tris(carbazol-9-yl)- triphenylamine (TCTA), 1,3-bis(carbazol-9-yl)benzene (mCP), 1,2,3,5-Tetrakis(carbazol-9-yl)-4,6-dicyanobenzene(4CZIPN),10-(2,12-Di-tert-butyl-5,9-dioxa-13b-boranaphtho[3,2,1-de]anthracen-7-yl)-9,9-dimethyl-9,10-dihydroacridine (TDBA–Ac), 1,3,5-Tri[(3-pyridyl)-phen-3-yl]benzene (TmPyPb), bis[2-(diphenylphosphino)phenyl]ether oxide (DPEPO), 4,7-diphenyl-1,10-phenanthrolin (Bphen), and Lithium fluoride (LiF).

Device fabrication: Devices were fabricated on patterned indium tin oxide (ITO, 135 nm) glass substrates with a sheet resistance of ~15 Ω/□. Firstly, ITO substrates were sequentially cleaned with ultra-sonication bath in alcohol, acetone and distilled water, and plasma. Then, the ITO substrates were loaded into a thermal deposition chamber with pressure of 5×10^{-4} Pa. Subsequently, DBR structures with TAPC and MoO3 with a doping ratio of 20 wt.% were co-evaporated. In DBR-OLEDs, the materials were deposited at a rate of 1-2 Å/s. The thickness was controlled using a quartz crystal monitor. The emitting area of all the hole-only devices and The emitting area of the OLEDs is determined by the overlap of two electrodes (5 mm × 2 mm). Each material source in chamber is equipped with a shutter for precise control. Preheating of MoO3 powder such that the material gas is released and held for 5 minutes. All the devices were transferred out for electrical measurement without encapsulation.

Characterization: Refractive index and extinction coefficient were measured with ellipsometer at 70° (Alpha SE, J. A.

Woollam Co. Ltd.), and the films were deposited on cleaned bare Si (100) substrates. Reflectance measured with angle-dependent spectrometer without polarizer (Fuxiang, R1), and the reference sample is quartz/silver (100 nm)/ZnS MgF2 (100 nm) mirror, set as 100%. The current-voltage characteristics, angle-dependent EL and OLED efficiency were measured with spectroradiometer equipment (McScience, Mc3000). All the measurements were carried out under ambient atmosphere.

Calculation and Simulation: The conductance σ is calculated with $\partial J/\partial V \times d$, where J is current density, V is driving voltage, and d is the film thickness. The electric field is equal to the driving voltage divided by the DBR thickness.

The optical simulations of DBR and OLED devices were performed by using a commercially available SETFOS (Fluxim) program. The refractive index, extinction coefficient (k), photoluminescence (PL) spectrum of emissive layers and thickness of each layer were used as input parameters. Transfer matrix method (TMM) and Gaussian dipole distribution dipole emitter as source are used in simulation.

4. CONCLUSIONS

In summary, we have co-evaporated oxide and organic material for low-reflective-index layer in constructing DBR, with MoO3 as the high-refractive-index layer. The conductive DBR exhibits excellent optical and electrical properties. The 8.5 pairs DBR shows a high reflectance of about 95% at 460 nm and a low driving voltage of 8.2 V at 100 mA $cm^{-2.}$ In addition, OLEDs with integrated conductive DBR structure demonstrated the function in optoelectronic applications. For the top-emitting blue device with DBR insertion, the turn-on voltage is as low as 4.2 V, and FWHM is reduced by half compared to that without DBR. Owing to the light confinement by DBR, the bottom emission of the device can be adjusted to the top emission. Therefore, the low deposition temperature of thermal evaporation paves the way for the fabrication of EL organic microcavities with non-metallic mirror leading to low values of FWHM, which is also a basic requirement for future electrically organic VCSELs.

REFERENCES

[1] Nakayama, T., Itoh, Y., Kakuta, A., "Organic photo‐and electroluminescent devices with double mirrors," Applied physics letters 63(5), 594-595(1993).

[2] Komikado, T., Inoue, A., Masuda, K., Ando, T., Umegaki S., "Multi-layered mirrors fabricated by spin-coating organic polymers," Thin Solid Films 515(7-8), 3887-3892(2007).

[3] Puzzo, D. P., Helander, M. G., O'Brien, P. G., Wang, Z., Soheilnia, N., Kherani, N., Lu, Z., Ozin, G. A., "Organic light-emitting diode microcavities from transparent conducting metal oxide photonic crystals," Nano letters 11(4), 1457-1462(2011).

[4] Bachevillier, S., Yuan, H. K., Strang, A., Levitsky, A., Frey, G. L., Hafner, A., Bradley, D. D. C., Stavrinou P. N., Stingelin, N., "Fully Solution‐Processed Photonic Structures from Inorganic/Organic Molecular Hybrid Materials and Commodity Polymers," Advanced Functional Materials 29(21), 1808152(2019).

[5] Daskalakis, K. S., Freire-Fernández, F., Moilanen, A. J., Van Dijken, S., Törmä, P., "Converting an organic light-emitting diode from blue to white with bragg modes," ACS photonics 6(11), 2655-2662(2019).

[6] Genco, A., Giordano, G., Carallo, S., Accorsi, G., Duan, Y., Gambino, S., Mazzeo, M., "High quality factor microcavity OLED employing metal-free electrically active Bragg mirrors," Organic Electronics 62, 174-180(2018).

[7] Dong, W. J., Lo, N. T., Jung, G. H., Ham, J., Lee, J. L., "Efficiency enhancement and angle-dependent color change in see-through organic photovoltaics using distributed Bragg reflectors," Applied Physics Letters 108, 103902(2016).

[8] Hong, K., Yu, H. K., Lee, I., Kim, S., Kim, Y., Kim, K., Lee, J. L., "Flexible top-emitting organic light emitting diodes with a functional dielectric reflector on a metal foil substrate," RSC Adv. 8, 26156–26160(2018).

[9] Iga, K., Koyama, F., Kinoshita, S., "Surface emitting semiconductor lasers," IEEE Journal of Quantum Electronics 24(9), 1845-1855(1988).

[10] Iga, K., "Vertical-Cavity Surface-Emitting Laser: Its Conception and Evolution," Jpn. J. Appl. Phys. 47(1R), 1(2008).

[11] Kajii, H., Yoshinaga, M., Karaki, T., Morifuji, M., Kondow, M., "Microcavity polymer electroluminescent devices with solution-processed dielectric distributed Bragg reflectors utilizing inorganic copper (I) thiocyanate and insulating polymers," Organic Electronics 88, 106011(2021).

[12] Ho, P. K., Stephen, D., Friend, R. H., Tessler, N., "All-polymer optoelectronic devices." science 285(5425), 233-236(1999).

[13] Yokoyama, D., Nakayama, K. I., Otani, T., Kido, J., "Wide‐Range Refractive Index Control of Organic Semiconductor Films Toward Advanced Optical Design of Organic Optoelectronic Devices," Adv. Mater. 24(47), 6368–6373(2012).

[14] Shi, X. B., Hu, Y., Wang, B., Zhang, L., Wang, Z. K., Liao, L. S., "Conductive Inorganic–Organic Hybrid Distributed Bragg Reflectors," Adv. Mater. 27(42), 6696–6701(2015).

[15] Lüssem B, Riede M, Leo K., "Doping of organic semiconductors." physica status solidi (a) 210(1),9-43(2013).

[16] Huang, J., Miller, P. F., Wilson, J. S., de Mello, A. J., de Mello, J. C., Bradley, D. D. C., "Investigation of the effects of doping and post‐deposition treatments on the conductivity, morphology, and work function of poly (3, 4‐ethylenedioxythiophene)/poly (styrene sulfonate) films," Advanced functional materials 15(2), 290-296 (2005).

[17] Chen, S. Y., Chu, T. Y., Chen, J. F., Su, C. Y., Chen, C. H., "Stable inverted bottom-emitting organic electroluminescent devices with molecular doping and morphology improvement," Applied physics letters 89(5), 053518 (2006).

[18] Angel, F. A., Wallace, J. U., Tang, C. W., "Effect of lithium and silver diffusion in single-stack and tandem OLED devices." Organic Electronics 42, 102-106 (2017).

[19] Park, M. H., Li, J. H., Kumar, A., Li, G., Yang, Y., "Doping of the metal oxide nanostructure and its influence in organic electronics," Advanced Functional Materials 19(8), 1241-1246 (2009).

[20] Lee, J. H., Kim, H. M., Kim, K. B., Kim, J. J., "Origin of charge generation efficiency of metal oxide p-dopants in organic semiconductors," Organic Electronics 12(6), 950-954 (2011).

[21] Salehi, A., Chen, Y., Fu, X., Peng, C., So, F., "Manipulating refractive index in organic light-emitting diodes," ACS applied materials & interfaces 10(11), 9595-9601 (2018).

[22] Boudaoud, L., Benramdane, N., Desfeux, R., Khelifa, B., Mathieu, C., "Structural and optical properties of MoO3 and V2O5 thin films prepared by Spray Pyrolysis," Catalysis today 113(3-4), 230-234 (2006).

[23] Kim, S. K., Jung, S.W., Park, H. U., Lampande, R., Kwon, J. H., "Accurate optical simulation method of tandem organic light-emitting diode with consideration of Purcell effect," Organic Electronics 95, 106192 (2021).

[24] Chen, Y. and Ma, D., "Organic semiconductor heterojunctions as charge generation layers and their application in tandem organic light-emitting diodes for high power efficiency," Journal of Materials Chemistry 22(36), 18718-18734 (2012).

[25] Schubert, S., Meiss, J., Müller‐Meskamp, L., Leo, K., "Improvement of transparent metal top electrodes for organic solar cells by introducing a high surface energy seed layer," Advanced Energy Materials 3(4), 438-443 (2013).